Available online at website: https://journal.bcrec.id/index.php/bcrec

Bulletin of Chemical Reaction Engineering & Catalysis, 20 (1) 2025, 64-77

Research Article

Pure Phase Nano Co_3O_4 Anchored on Nitrogen-Doped Porous Carbon for High-Performance Lithium-ion Batteries

Qingling Ruan[1], Zhehan Yang[1], Yan Liu[2], Junjie Xu[3,*], Jie Zhang[1], Jinhang Dai[1,*], Xingxing Gu[1,*]

[1]Chongqing Key Lab of Catalysis and Environments, School of Environment and Resources, Chongqing Technology and Business University, Chongqing 400067, P. R. China
[2]Information Technology Service Center of Zhongxian Industrial Park, Chongqing 404300, P. R. China
[3]Xi'an Rare Metal Materials Institute Co. Ltd, Xi'an 710000, P. R. China

Received: 29th October 2024; Revised: 15th January 2025; Accepted: 15th January 2025
Available online: 18th January 2025; Published regularly: April 2025

Abstract

Transition metal oxides (TMOs), due to their high theoretical capacity, and long cycling stability, have received increasing attention as the anode materials for lithium-ion batteries (LIBs). In this work, a kind of TMOs, Co_3O_4, anchored on nitrogen-doped porous carbon (NC), has been successfully synthesized via calcining cobalt salts and biomass precursor together. The synthesized Co_3O_4/NC as an anode material for lithium-ion batteries illustrates excellent cycling performances. At a current density of 1.0 $A.g^{-1}$, the Co_3O_4/NC anode could maintain a superior high reversible capacity of 1131.4 $mAh.g^{-1}$ after 2000 cycles. Even if the current increases to 8.0 $A.g^{-1}$, it still shows a reversible capacity of 502.9 $mAh.g^{-1}$. Such excellent electrochemical performances could be attributed to the high specific surface area of NC that facilitates the uniform dispersion of Co_3O_4 nanoparticles on it as well as the abundant porous structure and good conductivity of NC that enhance the Li^+ transfer and electrons transfer, respectively. In a word, this work provides a simple strategy for synthesizing the NC-supported pure phase Co_3O_4 composite anode material for realizing high-performance LIBs.

Keywords: Lithium-ion battery; high-performances; Nitrogen-doped porous carbon; Co_3O_4; anode

How to Cite: Ruan, Q., Yang, Z., Liu, Y., Xu, J., Zhang, J., Dai, J., Gu, X. (2025). Pure Phase Co_3O_4 Anchored on Nitrogen-Doped Porous Carbon for High-Performance Lithium-ion Batteries. *Bulletin of Chemical Reaction Engineering & Catalysis*, 20 (1), 64-77. (doi: 10.9767/bcrec.20238)

Permalink/DOI: https://doi.org/10.9767/bcrec.20238

Supporting Information (SI): https://journal.bcrec.id/index.php/bcrec/article/downloadSuppFile/20238/5607

1. Introduction

The increasing demand for green energy and sophisticated energy storage systems has prompted the advancement of lithium-ion batteries (LIBs) [1]. However, the traditional graphite anode has been unable to meet the rapid growth demand for the next generation of high-power and high-energy density lithium-ion batteries due to its low theoretical capacity (372 $mAh.g^{-1}$) [2]. Consequently, alternative anode materials with high rate performance and high capacity are being intensively investigated to develop a new generation of lithium-ion batteries [3]. In this context, transition metal oxides (TMOs) are regarded as the most promising anode materials, given their low cost, abundance in

* Corresponding Author.
Email: jie93guanaixin@163.com (Y. Xu)
jinhangdai@ctbu.edu.cn (J. Dai)
x.gu@ctbu.edu.cn (X. Gu)

natural resources, and theoretically high specific capacity [4]. Among various transition metal oxides (TMOs), cobalt(III) oxide (Co_3O_4) is considered to be one of the most promising anode materials because the 8-electron transfer reaction can provide a theoretical specific capacity of up to 890 $mAh.g^{-1}$ [5,6]. However, Co_3O_4 has two primary disadvantages: (i) the significant volume change of the active material results in electrode breakage and poor long-term cycle stability. (ii) The inherent low conductivity of Co_3O_4 results in poor rate performance [7]. These problems seriously hinder its practical application in LIBs.

To overcome the aforementioned obstacles and enhance the lithium storage capacity of Co_3O_4-based electrodes, researchers have conducted extensive research into two effective strategies. One strategy is the synthesis of distinctive Co_3O_4 nanostructures [8], such as nanoparticles [9,10], nanotubes [11,12], nanorods [13], nanosheets (NS) [14], nanoflowers [15] and hollow nanospheres [16]. These nanostructured Co_3O_4 with high surface area and small size is beneficial to the high contact area with the electrolyte and shorten the diffusion distance of lithium ions in the solid phase [17-19]. However, during the charge-discharge process, nanostructured Co_3O_4 still has many problems, such as serious agglomeration of Co_3O_4 particles and low conductivity. These problems will lead to electrode fracture, fast battery capacity decay, and poor long-term cycle stability and rate performance [20]. Therefore, the second strategy is focused on alleviating the agglomeration of Co_3O_4 and enhancing the conductivity. Introducing a specific conductive buffer matrix to form various Co_3O_4/carbon composites such as Co_3O_4/graphene [21], Co_3O_4/carbon nanotubes [22], Co_3O_4/carbon nanofibers [23], and Co_3O_4/porous carbon [18], is most popular nowadays. This is because carbon materials can provide fast electron conduction channels thereby enhancing the conductivity of active materials. Furthermore, it can provide a large specific surface area to alleviate Co_3O_4 agglomeration and mitigate the volume change during the charge-discharge cycle. Therefore, designing porous carbon-based materials with high specific surface area and abundant active sites to load nanostructured Co_3O_4 anode materials is an effective way to improve the electrochemical performance of lithium-ion batteries [24].

Inspired by the previous research, a new type of pure phase nanostructure Co_3O_4 anchored on porous nitrogen-doped carbon was successfully synthesized by a simple one-step calcination of ramie biomass waste with cobalt salt as shown in Figure 1. Compared with the previous two-step or multi-step work, this method is simple, fast, low cost, less pollution, and has potential industrial application prospects [25,26]. The resulting Co_3O_4/NC as the anode material in LIBs demonstrates excellent electrochemical performances, i.e., as high as 1131.4 $mAh.g^{-1}$ reversible capacity after 2000 cycles with a high coulombic efficiency (CE) of 99.88%. Such outstanding performances could be ascribed to the following advantages: (i) the nitrogen-doped carbon with good conductivity could improve the electrons transfer in Co_3O_4 based anode, thus enhancing its rate capability; (ii) the nano Co_3O_4 particles distributed on the NC surface uniformly, avoiding the agglomeration, which could reduce the diffusion distance of Li^+; (iii) abundant porous structure in NC could buffer the Co_3O_4 volume change during the cycle and be beneficial to the electrolyte infiltration, thus the cycling stability could be significantly enhanced.

2. Materials and Method

2.1 Materials

The ramie is harvest at Sichuan province. Anhydrous sodium carbonate, polyvinylidene fluoride (PVDF), N-methyl pyrrolidone (NMP), conductive carbon, and cobalt nitrate hexahydrate (99%) are purchased from Aladdin. The chemical reagents were not subjected to any further purification processes prior to use.

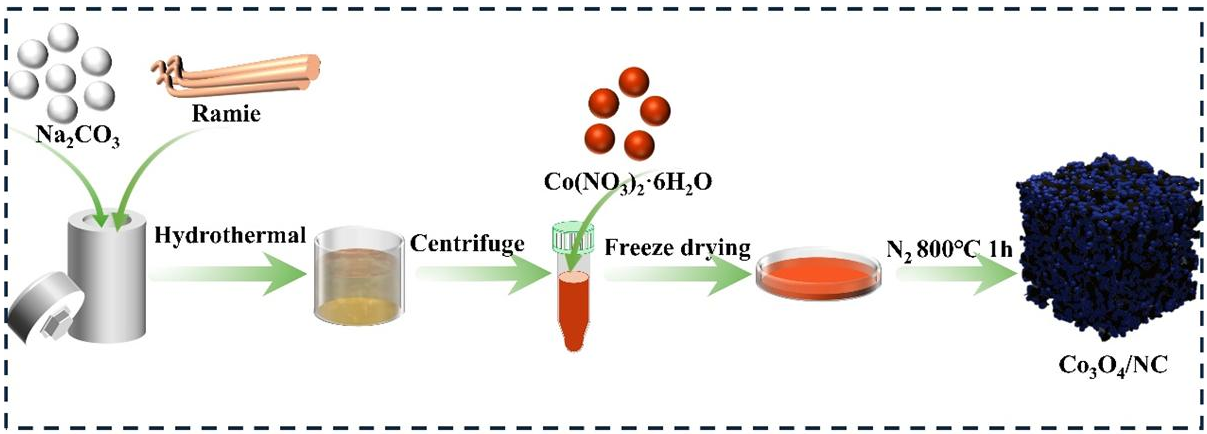

Figure 1. Preparation of Co_3O_4/NC.

2.2 Preparation of Co_3O_4/NC

0.7 g anhydrous sodium carbonate and 7 g ramie fiber were dispersed in 60 mL of distilled water, stirred for 30 min, and put into the reactor for heating at 115 °C for 30 min. After cooling, the supernatant was collected. Next, different amounts of cobalt salts were added into 40 mL supernatant, to form 0 mol/L, 0.05 mol/L, 0.1 mol/L, and 0.2 mol/L cobalt salts solutions. The solutions were freeze-drying for 48 hours to obtain the precursors. Then these precursors were calcined at 800 °C for 1 hour (at a rate of 5 °C.min^{-1}). After cooling, the calcined samples were washed with dilute HCl solution and distilled H_2O to neutral and finally dried to get the final samples.

2.3 Materials Characterizations

X-ray Diffraction (XRD, Rigaku, MiniFlex600) using Cu-Kα radiation was used to analyse the phase composition of the prepared materials. X-ray Photoelectron Spectroscopy (XPS, ThermoFisher Nexsa, USA) studied the surface chemical composition. JEM-F200 Transmission Electron Microscopy (TEM, JEOL) and FEI Quanta 250 FEG Scanning Electron Microscopy (SEM, USA) were used to perform morphology structures of the samples. N_2 adsorption-desorption isotherms were tested on V-Sorb 2800P to determine the specific surface areas (SSA) and pore volumes (PV) of the samples.

2.4 Electrochemical Measurements

To create a uniform slurry, active substances were combined with a conductive agent and binder in a 7:2:1 ratio. Subsequently the slurry was uniformly applied to copper foil and dried in oven. The CR2032 coin batteries were fabricated in an argon glove box, in which the prepared electrode and lithium foil were employed as the negative electrode and the counter electrode, respectively, the Celgard 2400 served as the separator, and the electrolyte consisted of 1 M $LiPF_6$ mixed in diethyl carbonate and fluoroethylene carbonate (EMC:FEC, 7:3, v/v). The electrolyte dosage of each battery was 30 µL. The LAND battery test system (LAND CT 2001A, China) was used to perform cycling and rate performance between 0.01-3.0 V at room temperature. Both the cyclic voltammetry (CV) and electrochemical impedance spectroscopy (EIS) measurements were recorded at CHI 660 electrochemical instrument.

2.5 Co_3O_4/NC and NC electrode's catalysis evaluation

For the study of catalytic activity, 5 mg of Co_3O_4/NC and NC were dispersed in 490:490 µL of water: ethanol by ultrasonication. Then 20 µL Nafion (5 wt %) is added to the solution and ultrasonically treated to obtain a uniform ink. The catalyst ink (5 µL) was loaded onto a glassy carbon (GC) electrode with a diameter of 3 mm and dried. Pt wire and Hg/HgO were used as counter electrode and reference electrode, respectively. O_2 was bubbled directly for at least an hour before measurement.

3. Results and Discussion

Firstly, the XRD characterizations were performed to identify the phase of the synthetic materials. As can be seen in Figure S1 and Figure 2a, without adding the cobalt source, only amorphous carbon could be observed with a wide peak at around 25°, which belongs to the (002) plane of the graphite structure, indicating that the obtained carbon material (NC) with partial graphitization [27]. When the added cobalt salt concentration is 0.05 mol/L, in addition to the XRD peak of amorphous carbon, there is also a diffraction peak belonging to elemental cobalt (JCPDS # 15-0806), therefore this sample is named Co/NC. When the added cobalt salt concentration is 0.1 mol/L, in addition to the XRD peak of amorphous carbon, there are only XRD peaks of Co_3O_4, corresponding to the crystal face of (111), (220), (311), (222), (400), (422), (511) and (440) of Co_3O_4 (JCPDS # 42-1467). And it should be noted that there are no complex peaks of elemental cobalt and other cobalt oxides, thus, this sample is named Co_3O_4/NC. When the added concentration further increases to 0.2 mol/L, in addition to the XRD peak of amorphous carbon and Co_3O_4, there appear the characterization peaks of CoO (JCPDS # 48-1719), corresponding to its crystal face of (200) and (220), therefore, this sample is named Co_3O_4@CoO/NC. According to the XRD analysis, it can be concluded that only when the cobalt salt concentration in the precursor is appropriate, the pure phase Co_3O_4 anchored on the nitrogen-doped carbon can be obtained.

Then the microstructure and morphology of the synthesized materials were further studied by SEM. As shown in Figure S2 and Figure 2b, both the NC and Co/NC samples demonstrate abundant 3D porous structures. The morphology of Co_3O_4/NC is distinctly different from that of NC and Co/NC. As shown in Figure 2c, it is hardly observed the porous structure of carbon, but it can be observed the Co_3O_4 nanoparticles are uniformly anchored on the surface of carbon and form unique 3D porous structures, which is because with the increase of cobalt source concentration, the pores of carbon are gradually filled, and the cobalt oxide gradually appears and even aggregate on the surface of the carbon. Particularly, the cobalt source concentration is too high, the aggregation becomes more and more serious, and finally, the

3D porous structure completely disappears as shown in Figure 2d. As is known, the nano-size and good dispersion of Co_3O_4 are beneficial to provide a larger specific surface area and shorten the transmission distance of electrons/lithium ions during charge and discharge [25]. The 3D porous structure also helps to adapt to the volume collapse of the active material and further maintains the integrity of the protective electrode material [28]. In order to further determine the porous structure and high specific surface area of Co_3O_4/NC, a nitrogen adsorption-desorption test was conducted. As shown in Figure S3a and Figure S3b, the specific surface area and pore volume of NC is 924.58 $m^2.g^{-1}$ and 0.53 $cm^3.g^{-1}$, respectively, with pore size of 2.27 nm. After the addition of a cobalt source, the samples' specific surface area, pore volume, and pore size gradually decreased as shown in Figure 2e and 2f. The Co_3O_4/NC sample still has a specific surface area of and pore volume of 87.86 $m^2.g^{-1}$ and 0.25 $cm^3.g^{-1}$, indicating its porous structures.

Based on the above results, the Co_3O_4/NC sample is the most promising candidate as the anode material for LIBs due to the pure phase of Co_3O_4 in the Co_3O_4/NC sample and higher theoretical specific capacity of Co_3O_4 compared to element Co and CoO, as well as the remained porous structure. Therefore, the XPS and TEM characterizations were further conducted for the Co_3O_4/NC sample. As shown in Figure 3a, from the full XPS spectrum of Co_3O_4/NC, it can be observed the peaks of C, N, O, and Co elements. The percentage of each element is shown in Table S1, in which the nitrogen and cobalt content is 1.29% and 28.53% respectively. In the high-resolution spectrum of C1s, there are obvious characteristic peaks of 284.8 eV, 289.12 eV, and 292.89 eV (Figure 3b), corresponding to C–C, C=O, and O=C–O, respectively, while the peak at 286.62 eV corresponds to C–N bond. Additionally, in the N1s high-resolution spectrum (Figure 3c), in addition to observing the peaks at 398.51 eV, 399.82 eV, and 400.8 eV for pyridine-N, pyrrole-N, and graphite-N, respectively, the C–N=C bond at 397.4 eV is also observed [29]. Both the C1s and N1s spectra indicate that the N atoms are doped into the carbon successfully [30]. From the O1s spectrum, except for the observation of the C=O bond at 531.2eV, the Co–O bond at 529.74eV is detected in the high-resolution spectra of O1s (Figure 3d), which should be ascribed to the existence of Co_3O_4 [26,31]. And the high-resolution Co2p spectrum further confirms the existence of Co_3O_4. As demonstrated in Figure 3e, one spin-orbit doublet of Co $2p_{3/2}$ can be divided into two deconvolution peaks of 780.5 eV and 779.2 eV, corresponding to Co^{2+} and Co^{3+}, and one spin-orbit doublet of Co $2p_{1/2}$ can also be divided into two deconvolution peaks of 794.29 and 795.61 eV, also corresponding to Co^{2+} and Co^{3+}, therefore, the Co_3O_4 indeed exist [32].

The TEM images of Co_3O_4/NC composites are shown in Figure 3f and Figure 3g. The red circle

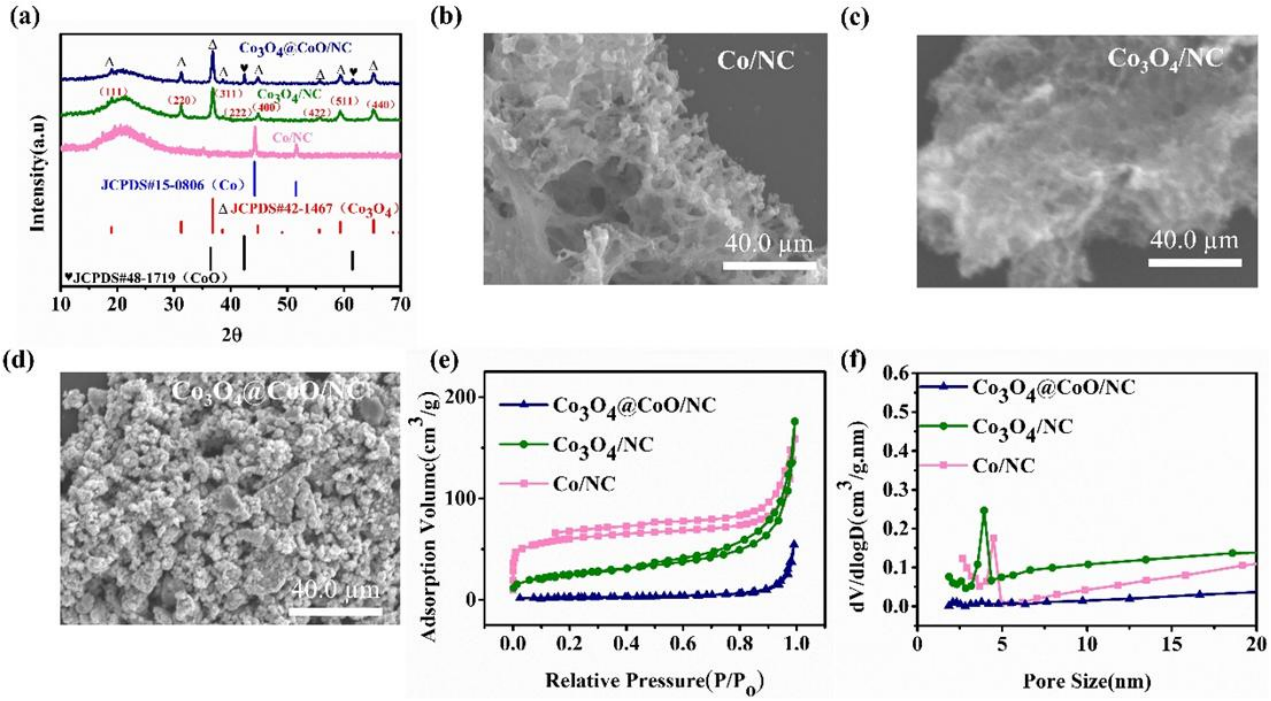

Figure 2. (a) The XRD patterns of Co/NC, Co_3O_4/NC, and Co_3O_4@CoO/NC. SEM images of (b) Co/NC, (c) Co_3O_4/NC, (d) Co_3O_4@CoO/NC. (e) N_2 adsorption-desorption isotherms of Co/NC, Co_3O_4/NC, and Co_3O_4@CoO/NC, (f) corresponding pore size distribution curves of Co/NC, Co_3O_4/NC, and Co_3O_4@CoO/NC.

in Figure 3f confirms there are many nanoparticles distributed on the surface of NC. Size further enlarged, it can be seen the (311) interplanar spacing (0.24 nm) of the Co_3O_4 phase as shown in Figure 3g, thus, the TEM characterization also proves the existence of nano-structured Co_3O_4 particles. The elemental mappings of the samples in Figure 3h-l show that C, N, O, and Co elements are uniformly distributed, further indicating the homogenous distribution of Co_3O_4 nanoparticles on the NC.

Then the lithium storage properties of NC and Co_3O_4/NC as anode materials for batteries were compared. The cyclic voltammetry (CV) curves of Co_3O_4/NC and NC electrodes in the potential range of 0.01-3.0 V at a scan rate of 0.1

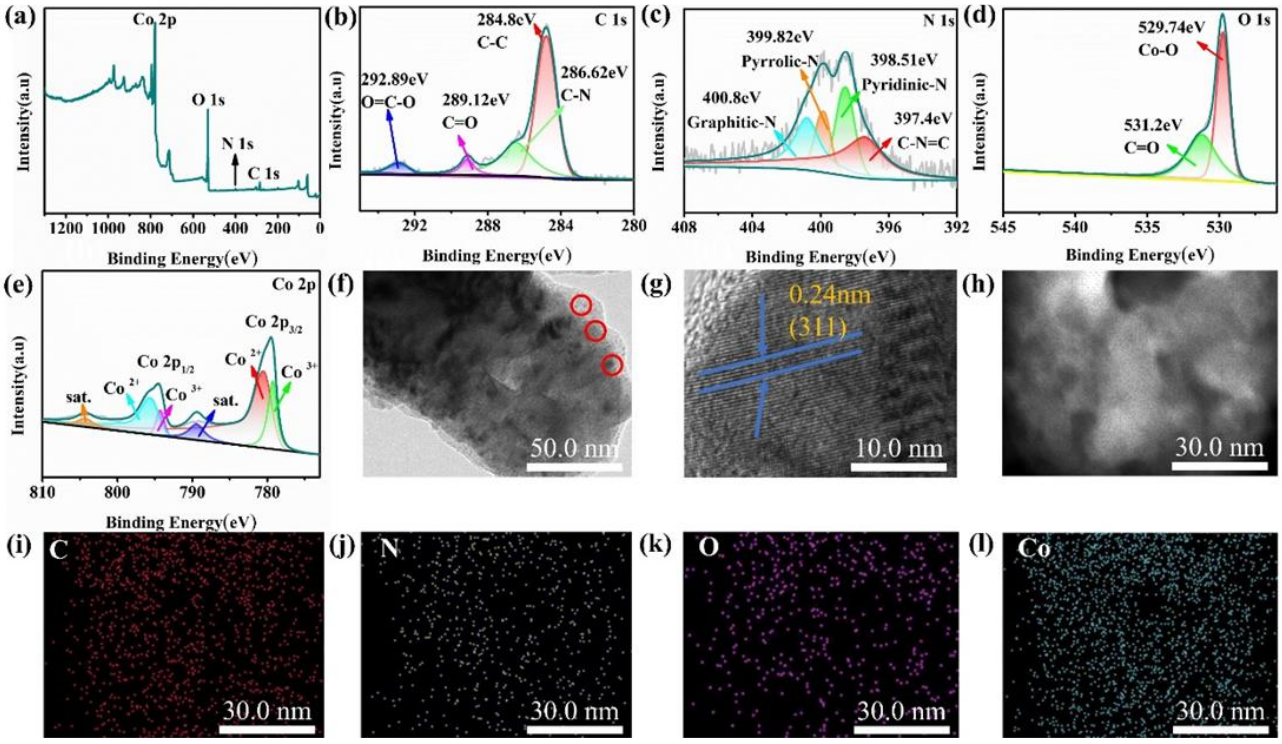

Figure 3. (a) Full XPS spectra of Co_3O_4/NC, (b) C1s, (c) N1s, (d) O1s, and (e) Co2p high-resolution XPS spectra of Co_3O_4/NC, (f-g) TEM images of Co_3O_4/NC sample. (h-l) Elemental mappings of C, N, O, and Co in Co_3O_4/NC.

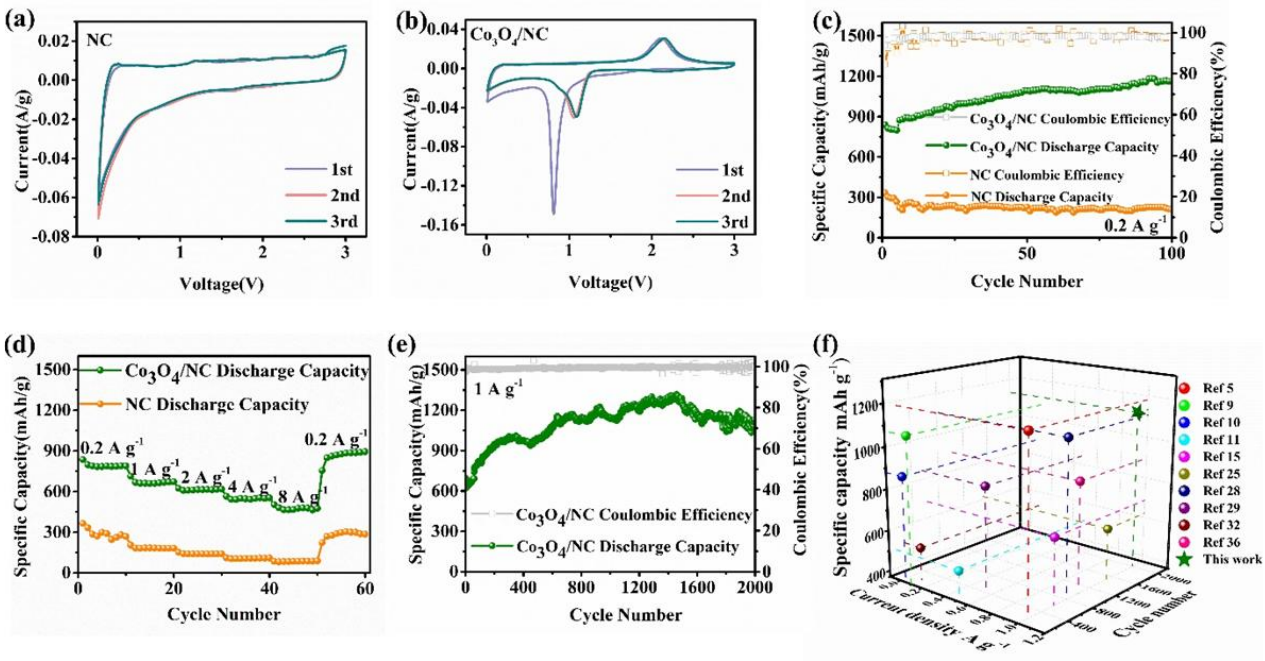

Figure 4. (a) Cyclic voltammetry curves of NC batteries, (b) Cyclic voltammetry curves of Co_3O_4/NC batteries, (c) Cycle performance of Co_3O_4/NC and NC batteries at a current density of 0.2 A.g^{-1}, (d) Rate performance curves of Co_3O_4/NC and NC batteries, (e) The cycle performance of Co_3O_4/NC batteries at a current density of 1 A.g^{-1}, (f) Comparison of cycle capacity with previous published works.

mV.s^{-1} are illustrated in Figure 4a and Figure 4b. As can be seen in Figure 4a, there are no obvious redox peaks in the CV curves for the NC electrode, which is the typical CV curve of an amorous carbon anode [26,33]. In contrast, the Co_3O_4/NC electrode (Figure 4b) showed a strong cathode peak at 0.80 V in the first cycle of the CV curve, which was due to the reduction of Co_3O_4 to elemental Co [34]. During the subsequent anodic scan, an oxidation peak appeared at 2.10 V, which can be attributed to the oxidation of elemental Co to Co_3O_4 [35]. From the second and third CV curves, it can be seen that the cathode peak for the reduction of Co_3O_4 to elemental Co has moved from 0.80 V to 1.05 V, which is possible because except the reduction of Co_3O_4, accompanying the decomposition of the electrolyte and the formation of SEI film on the electrode during the first cycle [36]. More importantly, from the second cycle, the redox peak positions remain basically unchanged, indicating good electrochemical reversibility [37]. Then the cycling performances for Co_3O_4/NC and NC electrodes at a low current of 0.2 A.g^{-1} are illustrated in Figure 4c. As can be seen, the Co_3O_4/NC illustrates an initial capacity of 839.8 mAh.g^{-1}, then the reversible capacity gradually increases to 1165.4 mAh.g^{-1} after 100 cycles, which is because of the reversible formation/dissolution of the SEI layer that contributes to the additional lithium storage [36]. During this charge/discharge voltage range, the NC electrode could only illustrate an initial capacity of 333.2 mAh.g^{-1} and a reversible capacity of 209.7 mAh.g^{-1}. Figure 4d shows the rate performance of Co_3O_4/NC and NC anodes. When the current density is 0.2 A.g^{-1}, 1 A.g^{-1}, 2 A.g^{-1}, 4 A.g^{-1}, and 8 A.g^{-1}, the reversible discharge capacities of Co_3O_4/NC batteries are 835.3, 712.7, 624, 565.2 and 502.9 mAh.g^{-1}, respectively, all higher than that of NC electrode. When the current density is restored to 0.2 A.g^{-1}, the discharge capacity is restored to 755.6 mAh.g^{-1}, approximately the initial capacity. This means that the Co_3O_4/NC electrode has excellent reversibility and rate capability. Therefore, the long-cycling stability of the Co_3O_4/NC electrode at high charge/discharge current (1 A.g^{-1}) is further investigated. As can be seen in Figure 4e, the Co_3O_4/NC anode demonstrates a superior high reversible capacity of 1134.1 mAh.g^{-1} after 2000 cycles. Such excellent electrochemical performances are better than many previous reports as shown in Figure 4f and Table S2. The electrochemical performance results prove the superior effect of uniform Co_3O_4 nanoparticle distribution on porous nitrogen-doped carbon, which is beneficial to realize high-performance LIBs.

In order to better understand why the Co_3O_4/NC electrode shows excellent performance.

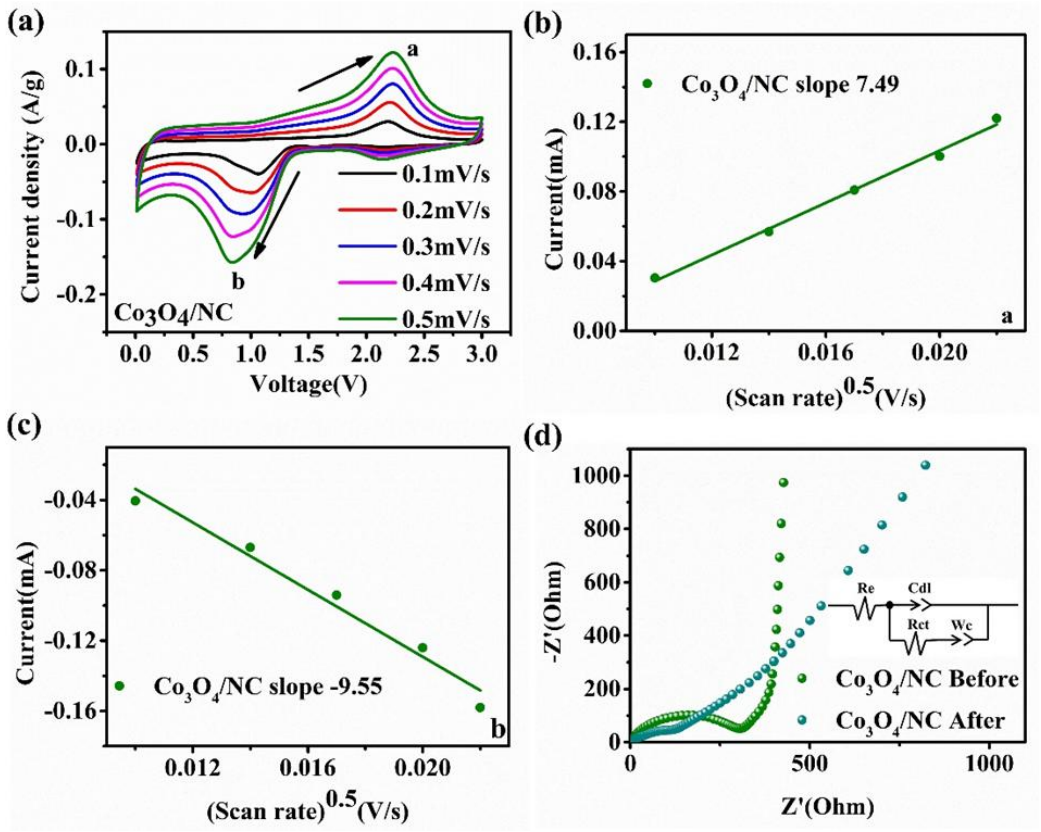

Figure 5. Lithium kinetics analysis: the CV curves of (a) Co_3O_4/NC electrodes at different scan rates (0.1-0.5 mV.s^{-1}), respectively. (b) Oxidation peak current vs. scan rate relationship; (c) Reduction peak current vs. scan rate relationship. (d) The Nyquist diagram of Co_3O_4/NC before and after 100 cycles and the equivalent circuit diagram of the battery.

The CV curves of the Co_3O_4/NC electrode at different scan rates (0.1 ~ 0.5 mv s^{-1}) were studied as illustrated in Figure 5a, which can be used to study the kinetics of Li^+ in the battery. The classical Randles-Sevcik equation can be used to calculate the diffusion coefficient of Li^+ [38]:

$$I_p = 2.69\times105n^{1.5}AD_{Li}^{0.5}C_{Li}v^{0.5} \text{ eq} \quad (1)$$

In the formula, n is the number of transferred electrons; I_p is the peak current; v is the scanning rate; C_{Li} is the concentration of Li^+; A is the electrode area for the reaction; D_{Li} is the diffusion rate of lithium ions.

According to the formula, peak current is linearly related to the square root of the scanning rate. Therefore, the linear plots of CV peak current (I_p) and $v^{0.5}$ are shown in Figure 5 (b) and Figure 5 (b). It can be seen that the Co_3O_4/NC anode has a relatively large slope in the whole redox reaction process. The larger the slope is, the larger the Li^+ diffusion coefficient is, and the faster the Li^+ diffusion rate is. The Li^+ diffusion coefficient in this work could reach as high as 1.01×10^{-11} and 1.29×10^{-11}, calculated based on the reduction and oxidation process, respectively, which are higher than 2-4 orders of magnitude compared with some previous reports as shown in Table S3. Then the EIS of Co_3O_4/NC electrode before cycling and after 500 cycles have been investigated. As shown in Figure 5d, no matter before cycling or after cycling 500 cycles, the EIS spectra demonstrate a semicircle and a slash, corresponding to the charge transfer resistance (*Rct*) and Warburg impedance (*Wc*) [39], respectively. According to the fitting model (inset of Figure 5d), the fitting results of *Rct* values are illustrated in Table S4. It can be seen that after 100 cycles, the *Rct* value of the Co_3O_4/NC electrode is 117.9 Ω, which is lower than that before the cycle (310.2 Ω). The charge transfer resistance decreases with the increase of the number of charge and discharge cycles, which is in good agreement with the cycle results. The good kinetics of the Co_3O_4/NC electrode can be attributed to the good conductivity of NC and its porous structure can accommodate volume expansion to ensure the integrity of the entire electrode.

The electrode with good kinetics has good catalytic activity. Thus, finally, in a standard three-electrode system, cyclic voltammetry (CV) and linear sweep voltammetry (LSV) were used to study the catalytic activity of Co_3O_4/NC and NC catalysts in O_2-saturated 1 M KOH electrolyte solution. As shown in Figure S4a, the reduction peak for oxygen reduction reaction by Co_3O_4/NC catalyst is more obvious than that using NC catalyst, and the reduction peak potential position is more positively for Co_3O_4/NC catalyst, indicating that Co_3O_4/NC has better catalytic performance than NC [40]. Then the LSV diagram in Figure S4b shows the HER activity comparison between Co_3O_4/NC and NC in the range of 0 to − 2.5 V. The onset potential of Co_3O_4/NC (−1.37 V) is slightly lower than that of NC (− 1.5 V), indicating Co_3O_4/NC has better catalyzing property on HER [12,40]. While the LSV curves for OER characterization are illustrated in Figure S4c, it can be clearly observed that the onset potential of NC is 1.45 V, but the onset potential of Co_3O_4/NC is only 0.63 V. The onset potential of Co_3O_4/NC is lower than that of NC, also indicating Co_3O_4/NC has better catalyzing properties for OER [40]. In a word, the above results show that nano-Co_3O_4/NC exhibits better catalytic performance than NC in hydrogen and oxygen evolution reactions.

4. Conclusion

In this work, pure-phase Co_3O_4 nanoparticles anchored on the porous nitrogen-doped carbon have been successfully synthesized by simply pyrolysis of the cost-effective waste biomass and cobalt salt. Due to the uniform distribution of Co_3O_4 nanoparticles and the good conductivity of NC, the inherent low conductivity of Co_3O_4 is improved. The rich porous structure alleviates the volume change and ensures the electrode integrity and long-term cycle stability. The synthesized Co_3O_4/NC composite anode exhibits excellent cycle stability and rate performance, that is, after 2000 cycles, the capacity at 1A.g^{-1} is 1134.1 mAh.g^{-1}. In a word, this work provides a facile and available strategy to synthesize high-performance TMO-based anode materials for LIBs.

Acknowledgment

This study was funded by the National Natural Science Foundation of China (Grant No.51902036), Natural Science Foundation of Chongqing Science & Technology Commission (Grant No. CSTB2022NSCQ-MSX0828), the Key Science and Technology Research Program of Chongqing Education Commission (No. KJZD-K202200807), Chongqing Bayu Scholars Support Program (No. YS2022050) and Research Project of Innovative Talent Training Engineering Program of Chongqing Primary and Secondary School (Grant No. CY240806).

CRedit Author Statement

Qingling Ruan: Method, Resources, Data Curation, writing original draft, editing and reviewing; Zhehan Yang: Supervision; Yan Liu: writing; Junjie Xu: Review and Editing, Supervision; Jie Zhang: Review and Editing, Supervision; Jinhang Dai: Review and Editing, Supervision; Xingxing Gu: Writing, Review and Editing, Supervision, Project administration, Funding acquisition.

Conflict of interest

There is no interest in competition.

References

[1] Song, D., Yu, J., Wang, M., Tan, Q., Liu, K., Li, J. (2023). Advancing recycling of spent lithium-ion batteries: From green chemistry to circular economy. *Energy Storage Materials,* 102870. DOI: 10.1016/j.ensm.2023.102870

[2] Xu, J., Cai, X., Cai, S., Shao, Y., Hu, C., Lu, S., Ding, S. (2023). High-energy lithium-ion batteries: recent progress and a promising future in applications. *Energy & Environmental Materials*, 6 (5), e12450. DOI: 10.1002/eem2.12450

[3] Chang, H., Wu, Y.-R., Han, X., Yi, T.-F. (2021). Recent developments in advanced anode materials for lithium-ion batteries. *Energy Materials,* 1 (1), 100003. DOI: 10.20517/energymater.2021.02

[4] Cao, Y., He, Y., Gang, H., Wu, B., Yan, L., Wei, D., Wang, H. (2023). Stability study of transition metal oxide electrode materials. *Journal of Power Sources*, 560 (15), 232710. DOI: 10.1016/j.jpowsour.2023.232710

[5] Xiao, Y., Li, T., Mao, Y., Hao, X., Wang, W., Meng, S., Wu, J., Zhao, J. (2023). Core-shell N-doped carbon embedded Co_3O_4 nanoparticles with interconnected and hierarchical porous structure as superior anode materials for lithium-ion batteries. *Journal of Energy Storage*, 63, 106998. DOI: 10.1016/j.est.2023.106998

[6] Roselin, L.S., Juang, R.-S., Hsieh, C.-T., Sagadevan, S., Umar, A., Selvin, R., Hegazy, H.H. (2019). Recent advances and perspectives of carbon-based nanostructures as anode materials for Li-ion batteries. *Materials*, 12 (8), 1229. DOI: 10.3390/ma12081229

[7] Wang, L., Chen, B., Ma, J., Cui, G., Chen, L. (2018). Reviving lithium cobalt oxide-based lithium secondary batteries-toward a higher energy density. *Chemical Society Reviews*, 47(17), 6505-6602. DOI: 10.1039/C8CS00322J

[8] Zhao, Y., Wang, L.P., Sougrati, M.T., Feng, Z., Leconte, Y., Fisher, A., Srinivasan, M., Xu, Z. (2017). A review on design strategies for carbon based metal oxides and sulfides nanocomposites for high performance Li and Na ion battery anodes. *Advanced Energy Materials*, 7(9), 1601424. DOI: 10.1002/aenm.201601424

[9] Mahmood, Z.H., Jarosova, M., Kzar, H.H., Machek, P., Zaidi, M., Dehno Khalaji, A., Khlewee, I.H., Altimari, U.S., Mustafa, Y.F., Kadhim, M.M. (2022). Synthesis and characterization of Co_3O_4 nanoparticles: application as performing anode in Li-ion batteries. *Journal of the Chinese Chemical Society*, 69 (4), 657-662. DOI: 10.1002/jccs.202100525

[10] Wang, D., Yu, Y., He, H., Wang, J., Zhou, W., Abruña, H.D. (2015). Template-free synthesis of hollow-structured Co_3O_4 nanoparticles as high-performance anodes for lithium-ion batteries. *ACS Nano*, 9 (2), 1775-1781. DOI: 10.1021/nn506624g

[11] Liu, W., Fu, Y., Li, Y., Chen, S., Song, Y., Wang, L. (2019). Three-dimensional carbon foam surrounded by carbon nanotubes and Co-Co_3O_4 nanoparticles for stable lithium-ion batteries. *Composites Part B: Engineering*, 163, 464-470. DOI: 10.1016/j.compositesb.2019.01.038

[12] Li, S., Wu, K., Li, L., Suo, L., Zhu, Y. (2019). An architecture of dandelion-type Ni-Co_3O_4 microspheres on carbon nanotube films toward an efficient catalyst for oxygen reduction in zinc-air batteries. *Applied Surface Science*, 481, 40-51. DOI: 10.1016/j.apsusc.2019.03.053

[13] Li, X., Tian, X., Yang, T., Song, Y., Liu, Y., Guo, Q., Liu, Z. (2018). Two-pot synthesis of one-dimensional hierarchically porous Co_3O_4 nanorods as anode for lithium-ion battery. *Journal of Alloys and Compounds*, 735, 2446-2452. DOI: 10.1016/j.jallcom.2017.12.001

[14] Sennu, P., Madhavi, S., Aravindan, V., Lee, Y.-S. (2020). Co_3O_4 nanosheets as battery-type electrode for high-energy Li-ion capacitors: a sustained Li-storage via conversion pathway. *ACS Nano*, 14 (8), 10648-10654. DOI: 10.1021/acsnano.0c04950

[15] Zhang, Y., Xie, M., He, Y., Zhang, Y., Liu, L., Hao, T., Ma, Y., Shi, Y., Sun, Z., Liu, N. (2021). Hybrid NiO/Co_3O_4 nanoflowers as high-performance anode materials for lithium-ion batteries. *Chemical Engineering Journal*, 420, 130469. DOI: 10.1016/j.cej.2021.130469

[16] Xiong, S., Lin, M., Wang, L., Liu, S., Weng, S., Jiang, S., Xu, Y., Jiao, Y., Chen, J. (2021). Defects-type three-dimensional Co_3O_4 nanomaterials for energy conversion and low temperature energy storage. *Applied Surface Science*, 546, 149064. DOI: 10.1016/j.apsusc.2021.149064

[17] Hu, C., Dai, L. (2019). Doping of carbon materials for metal-free electrocatalysis. *Advanced Materials*, 31(7), 1804672. DOI: 10.1002/adma.201804672

[18] Liu, H., Liu, X., Li, W., Guo, X., Wang, Y., Wang, G., Zhao, D. (2017). Porous carbon composites for next generation rechargeable lithium batteries. *Advanced Energy Materials*, 7(24), 1700283. DOI: 10.1002/aenm.201700283

[19] Rehnlund, D., Wang, Z., Nyholm, L. (2022). Lithium-diffusion induced capacity losses in lithium-based batteries. *Advanced Materials*, 34(19), 2108827. DOI: 10.1002/adma.202108827

[20] Gu, Z.-Y., Sun, Z.-H., Guo, J.-Z., Zhao, X.-X., Zhao, C.-D., Li, S.-F., Wang, X.-T., Li, W.-H., Heng, Y.-L., Wu, X.-L. (2020). High-rate and long-cycle cathode for sodium-ion batteries: Enhanced electrode stability and kinetics via binder adjustment. *ACS Applied Materials & Interfaces*, 12 (42), 47580-47589. DOI: 10.1021/acsami.0c14294

[21] Reddy, Y.V.M., Shin, J.H., Palakollu, V.N., Sravani, B., Choi, C.-H., Park, K., Kim, S.-K., Madhavi, G., Park, J.P., Shetti, N.P. (2022). Strategies, advances, and challenges associated with the use of graphene-based nanocomposites for electrochemical biosensors. *Advances in Colloid and Interface Science*, 304, 102664. DOI: 10.1016/j.cis.2022.102664

[22] Sehrawat, P., Julien, C., Islam, S. (2016). Carbon nanotubes in Li-ion batteries: A review. *Materials Science and Engineering: B*, 213, 12-40. DOI: 10.1016/j.mseb.2016.06.013

[23] Li, W., Li, M., Adair, K.R., Sun, X., Yu, Y. (2017). Carbon nanofiber-based nanostructures for lithium-ion and sodium-ion batteries. *Journal of Materials Chemistry A*, 5(27), 13882-13906. DOI: 10.1039/C7TA02153D

[24] Zheng, M., Tang, H., Li, L., Hu, Q., Zhang, L., Xue, H., Pang, H. (2018). Hierarchically nanostructured transition metal oxides for lithium-ion batteries. *Advanced Science*, 5 (3), 1700592. 1700592. DOI: 10.1002/advs.201700592

[25] Zhang, M., Deng, Z.-P., Zhang, X.-F., Huo, L.-H. Gao, S. (2021). Biomass-derived graphitic carbon/Co_3O_4 nanocomposites with pseudocapacitance for lithium storage. *ACS Applied Nano Materials*, 4(2), 1340-1350. DOI: 10.1021/acsanm.0c02903

[26] Han, Q., Li, Y., Zhang, W., Li, X., Geng, D., Zhang, X., He, D. (2019). Two-step route for manufacturing the bio-mesopores structure functional composites by mushroom-derived carbon/Co_3O_4 for lithium-ion batteries. *Journal of Electroanalytical Chemistry*, 848, 113347. DOI: 10.1016/j.jelechem.2019.113347

[27] Lee, J.S., Jo, M.S., Saroha, R., Jung, D.S., Seon, Y.H., Lee, J.S., Kang, Y.C., Kang, D.W., Cho, J.S. (2020). Hierarchically well-developed porous graphene nanofibers comprising N-doped graphitic C-coated cobalt oxide hollow nanospheres as anodes for high-rate Li-ion batteries. *Small*, 16 (32), 2002213. DOI: 10.1002/smll.202002213

[28] Zhai, X., Xu, X., Zhu, X., Zhao, Y., Li, J., Jin, H. (2018). Porous layer assembled hierarchical Co_3O_4 as anode materials for lithium-ion batteries. *Journal of Materials Science*, 53, 1356-1364. DOI: 10.1007/s10853-017-1579-3

[29] Ge, Z., Jiang, L., Liang, F., Zhang, Z., Wu, D., Ye, W., Han, N., Rui, Y., Zhang, W., Tang, B.J.E. (2022). Nitrogen-doped porous Ag–C@ Co_3O_4 nanocomposite for boosting lithium ion batteries. *Energy & Fuels*, 36(5), 2861-2871. DOI: 10.1021/acs.energyfuels.1c04338

[30] Liu, K., Xiong, X., Li, J., Liu, M., Wu, Z.,Li, F. (2024). Controlled graphene interfacial carbon nitride preparation for carbon negative electrodes of lithium-ion batteries. *Electrochimica Acta,* 493,1 44219. DOI: 10.1016/j.electacta.2024.144219

[31] Han, X., Ang, E.H., Zhou, C., Zhu, F., Zhang, X., Geng, H., Cao, X., Zheng, J., Gu, H. (2021). Dual carbon-confined Sb_2 Se_3 nanoparticles with pseudocapacitive properties for high-performance lithium-ion half/full batteries. *Dalton Transactions*, 50 (19), 6642-6649. DOI: 10.1039/D1DT00025J

[32] Hou, Z., Shu, C., Hei, P., Yang, T., Zheng, R., Ran, Z., Long, J. (2020). A 3D free-standing Co doped Ni_2P nanowire oxygen electrode for stable and long-life lithium–oxygen batteries. *Nanoscale*, 12 (12), 6785-6794. DOI: 10.1039/C9NR10793B

[33] Guo, L., Ding, Y., Qin, C., Li, W., Du, J., Fu, Z., Song, W., Wang, F. (2016). Nitrogen-doped porous carbon spheres anchored with Co_3O_4 nanoparticles as high-performance anode materials for lithium-ion batteries. *Electrochimica Acta,* 187, 234-242. DOI: 10.1016/j.electacta.2015.11.065

[34] Zhong, W., Zeng, Z., Cheng, S., Xie, J. (2024). Advancements in Prelithiation Technology: Transforming Batteries from Li-Shortage to Li-Rich Systems. *Advanced Functional Materials*, 34(2), 2307860. DOI: 10.1002/adfm.202307860

[35] Li, L., Dong, G., Xu, Y., Cheng, X., Gao, S., Zhang, X., Zhao, H., Huo, L. (2020). H_3IDC-assisted synthesis of mesoporous ultrafine Co_3O_4/N-doped carbon nanowires as a high rate and long-life anode for Lithium-ion batteries. *Journal of Alloys and Compounds*, 818, 152826. DOI: 10.1016/j.jallcom.2019.152826

[36] Kang, Y., Zhang, Y.-H., Shi, Q., Shi, H., Xue, D., Shi, F.-N. (2021). Highly efficient Co_3O_4/CeO_2 heterostructure as anode for lithium-ion batteries. J*ournal of Colloid and Interface Science*, 585, 705-715. DOI: 10.1016/j.jcis.2020.10.050

[37] Wang, Y., Guo, R., Liu, W., Zhu, L., Huang, W., Wang, W., Zheng, H. (2019). Co_3O_4 nanospheres composed of highly interconnected nanoparticles for boosting Li-Ion storage. *Journal of Power Sources*, 444, 227260. DOI: 10.1016/j.jpowsour.2019.227260

[38] Ma, S., Wan, G., Yan, Z., Liu, X., Chen, T., Wang, X., Dai, J., Lin, J., Liu, T., Gu, X. (2024). Eco-friendly aqueous binder derived from waste ramie for high-performance Li-S battery. 109853. *Chinese Chemical Letters*, 109853. DOI: 10.1016/j.cclet.2024.109853

[39] Li, J., Dou, F., Gong, J., Gao, Y., Hua, Y., Sielicki, K., Zhang, D., Mijowska, E., Chen, X. J. (2023). Recycling of plastic wastes for the mass production of yolk–shell-nanostructured Co_3O_4@C for lithium-ion batteries. *ACS Applied Nano Materials*, 6(2), 1171-1180. DOI: 10.1021/acsanm.2c04757

[40] Sennu, P., Christy, M., Aravindan, V., Lee, Y., Nahm, K., Lee, Y. (2015). Two-Dimensional Mesoporous Cobalt Sulfide Nanosheets as a Superior Anode for a Li-Ion Battery and a Bifunctional Electrocatalyst for the Li-O_2 System. *Chemistry of Materials*, 27 (16), 5726e5735. DOI: 10.1021/acs.chemmater.5b02364